Chaos

A cellular automata model for expanding turbulent flames

Cite as: Chaos **30**, 113141 (2020); https://doi.org/10.1063/5.0018947
Submitted: 18 June 2020 . Accepted: 28 October 2020 . Published Online: 23 November 2020

Vishnu R. Unni, Chung K. Law, and Abhishek Saha

A cellular automata model for expanding turbulent flames

Cite as: Chaos **30**, 113141 (2020); doi: 10.1063/5.0018947
Submitted: 18 June 2020 · Accepted: 28 October 2020 ·
Published Online: 23 November 2020

Vishnu R. Unni,[1,a)] Chung K. Law,[2] and Abhishek Saha[1,a)]

AFFILIATIONS

[1]Department of Mechanical and Aerospace Engineering, University of California San Diego, La Jolla, California 92093, USA
[2]Department of Mechanical and Aerospace Engineering, Princeton University, Princeton, New Jersey 08544, USA

[a)]**Authors to whom correspondence should be addressed:** vunni@eng.ucsd.edu and asaha@eng.ucsd.edu

ABSTRACT

Cellular automata models based on population dynamics, introduced by Von Neumann in the 1950s, has been successfully used to describe pattern development and front propagation in many applications, such as crystal growth, forest fires, fractal growth in biological media, etc. We, herein, explore the possibility of using a cellular automaton, based on the population dynamics of flamelets, as a low-order model to describe the dynamics of an expanding flame propagating in a turbulent environment. A turbulent flame is constituted by numerous flamelets, each of which interacts with their neighborhood composed of other flamelets, as well as unburned and burnt fluid particles. This local interaction leads to global flame dynamics. The effect of turbulence is simulated by introducing stochasticity in the local interaction and hence in the temporal evolution of the flamefront. Our results show that the model preserves various multifractal characteristics of the expanding turbulent flame and captures several characteristics of expanding turbulent flames observed in experiments. For example, at low turbulence levels, an increase in global burning rate leads to an increase in the turbulence level, while beyond a critical turbulence level, the expanding flame becomes increasingly fragmented, and consequently, the total burning rate decreases with increasing turbulence. Furthermore, at an extremely high turbulence level, the ignition kernel quenches at its nascent state and consequently loses its ability to propagate as an expanding flame.

Propagation and stability of turbulent flames, which have immense importance in performance, efficiency, and reliability of power generating devices, strongly depend on the interactions between turbulence and flamefront. Such non-linear interaction causes changes in characteristics of flamefront morphology, which could also lead to critical events like local or global extinction of the flame, ceasing the operation of the device. Inherent non-linear coupling between flow and flame chemistry renders modeling such dynamics of flow-flame interaction complex, and as such, development of lower order models is necessary. Cellular automata have been used for modeling the interaction of various complex systems. In this paper, we introduce a low-order model based on cellular automata that captures the evolving topology of an expanding flamefront in a turbulent flow. We show the qualitative equivalence between the dynamics exhibited by the model and that was observed from experiments by examining the multifractal nature of the topology of the flamefront at various conditions.

I. INTRODUCTION

A premixed flame, propagating in a turbulent environment, undergoes continuous unsteady straining by eddies at various scales, resulting in wrinkled flamefront and enhanced transport.[1,2] The combined effect alters both global (burning rate, flame morphology) and local (flame stretching, extinction, re-ignition) dynamics of the premixed flame. The local propagation of the flamelets that collectively constitute the global turbulent flame propagation is subjected to nonlinear effects caused by the inherent unsteadiness in the flow and front geometry.[3–6] Moreover, enhanced mixing induced by turbulence can promote or inhibit local flame propagation by either replenishing or depleting the fresh mixture at the flamefront. The interaction between flame and turbulence can become even more complicated if the flame is further subjected to inherent cellular instabilities. Two of the well-known cellular instabilities are the Darrieus–Landau hydrodynamic instability, which is caused by the sharp density gradient across the flamefront, and diffusional–thermal cellular instability, which is triggered by stronger

mass diffusion relative to thermal diffusion in mixtures with subunity Lewis number (*Le*). Through the generation of cellular structures and additional surface area, these instabilities can supplement or negate the effects of turbulence on flame propagation.[7–11] Owing to these interactions between the various hydrodynamic and transport effects with the reacting propagating flamefront, turbulent combustion is inherently complex and challenging to model.

This complexity in the dynamics of a turbulent flame essentially arises from the local interactions in a turbulent reactive field. In the simplistic sense, a turbulent flame can be described as a collection of flamelets that interact with their neighborhood containing fluid particles constituting burned or unburned, reactive mixture as well as other flamelets. Here, a flamelet is a hydrodynamically thin diffusive–reactive interfacial region within which chemical energy is converted to thermal energy. The relative distribution of fluid particles of different dynamic states (such as burned, unburned, burning, etc.) dictates the local interaction in the reaction field and thus determines the population dynamics of the flamelets and hence the global evolution of the flamefront. Such a system wherein local interactions among the constituents of the system lead to emergence of a global dynamics, also known as a collective behavior, is called a complex system. Recognizing that other complex systems such as social networks, global economy, climatic system, school of fish, ant colony, etc., are often modeled using cellular automata,[12] in this work, we explore the feasibility of adapting such a model to describe the propagation of turbulent premixed flames.

Cellular automaton is a mathematical machinery that provides a natural framework to model dynamics of complex systems. In general, a cellular automaton consists of a number of cells distributed in regular or irregular grids, and with each cell assuming a particular state. Each cell interacts with its neighboring cells following a set of rules leading to temporal evolution of their states. Such local interactions cause emergence of the global dynamics in a cellular automaton akin to the emergence of collective behavior in a complex system.[12]

Cellular automata have been previously used to study combustion systems,[13–15] particularly to quantitatively estimate the propagation speed of turbulent flames using the knowledge of laminar flame propagation speed. On the contrary, the objective of this study is to consider a turbulent flame as a propagating front in a complex system and to develop a low-order model based on the population dynamics of flamelets, in the framework of a cellular automaton that qualitatively describes the dynamics of a turbulent flame. Our focus will be primarily on studying the characteristics of the topology of a propagating turbulent flamefront. Although the model can be extended to other geometries, in this study, we have used an expanding flame configuration, since it has been extensively studied experimentally for a wide range of pressures, temperatures, and turbulence levels.[7,8,16–21] We will show that this simple model is able to capture various dynamics reported in experiments conducted on expanding turbulent flames and also predicts the fractal behavior exhibited by an expanding turbulent flamefront when subjected to various levels of turbulence.

In the following, we will first introduce the framework for the cellular automata based population dynamics model to be used for propagating turbulent flame in Sec. II. Subsequently, in Sec. III, we present the key features, flame dynamics, and multifractal characteristics of expanding turbulent flames captured by the model and compare them with the previous experimental findings.

II. THE POPULATION DYNAMICS MODEL FOR FLAME PROPAGATION

In a premixed turbulent flame, the flamelets that constitute the wrinkled flamefront interact with their surrounding fluid particles and such local interactions result either in a local propagation or quenching of the flamelet. The propagation and quenching events alter both the total population of flamelets in the reaction field and their spatial distribution, which in turn dictate the instantaneous flame propagation speed.[22] We define a probabilistic cellular automaton to model this population dynamics of flamelets in an expanding turbulent flame. For simplicity, in this study, we consider a 2D reaction zone containing premixed reactants. The reaction field is divided into a regular hexagonal grid, where each of the cells of the grid houses a gas parcel. The length of the side of each hexagonal cell is l and it corresponds to the smallest scale of the flamelets present in the turbulent reactive flow, which is of the order of the flame thickness. We assume that the gas parcels in each of the cells can be in either one of three states. State 1: unburned gas parcel; State 2: burning gas parcel or flamelet; and State 3: burned gas parcel. At time $t = 0$, the cells in the entire domain of the hexagonal grid is in State 1, representing a reactive field filled with the unburned combustible mixture. In the next time step of the cellular automaton, n cells at the center of the hexagonal grid is transformed to State 2 consisting of flamelets. This corresponds to the formation of a nascent flame kernel through spark ignition at the center of the domain. In the current study, n is arbitrarily chosen to be 7. Once ignited, the flamelets at the center of the hexagonal grid propagate out according to the following rules of cellular automaton. Here, it is noted that the value of n corresponds to the energy of the ignition kernel created by the spark generally used for initiation of a premixed flame, and that the propagation of the flame, once it develops into a stable flamefront, is insensitive of the value of n.

The rules for the evolution of the cellular automata are summarized in Fig. 1. A flamelet (State 2) is converted to a burned gas parcel (State 3) in the next step of cellular automaton, as we would expect in the case of flame propagation through complete combustion. An unburned gas parcel (State 1) is converted to a flamelet (State 2) with a probability $Q = 1 - P$ if the unburned gas parcel is surrounded by at least one flamelet. This rule corresponds to the process of flame propagation as a result of local diffusion of heat and reactive species. Here, the probability P is introduced to account for turbulence in the reaction field. Despite the presence of flamelet in the neighborhood of an unburned gas parcel, turbulent fluctuations can introduce high local strain across two gas parcels preventing flame propagation from the flamelet to a neighboring unburned gas parcel. Moreover, in such locations where a flamelet fails to propagate into the unburned gas, turbulence can cause unburned gas parcels to enter into locations where a burned gas parcel is present and vice versa, with a probability, R. Physically, these two rules introduce events, such as local extinction, re-ignition, and wrinkling of the flamefronts, which are characteristics of turbulent flames. In order to simplify the model, for this study, we assumed these two

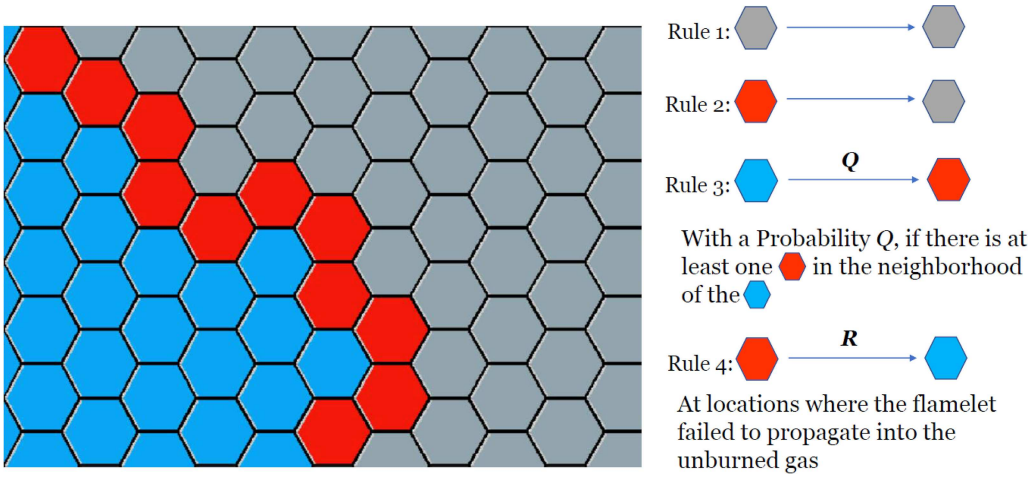

FIG. 1. Rules for evolution of the cellular automata. Color codes: blue: unburned; red: burning; and gray: burned.

probabilities to be equal, i.e., $R = Q$. Rest of the locations where burned gas parcels are present continue to have a burned gas parcel. Note that the wrinkling increases as P increases. The proposed model only simulates the effect of a front propagation in a turbulent environment and in its present form does not capture other effects, such as flamefront instabilities that may cause additional wrinkling of the flame.

The mathematical algorithm to describe this cellular automata is defined as follows. We consider A^k to be a matrix representing the grid of fluid parcels at time instant k. In a two-dimensional grid, A^k_{ij} represents the state of a fluid parcel at location (i,j) at time instant k. Note that in this study, the physical position of (i,j) is appropriately chosen such that fluid parcel corresponding to $A^k_{i,j}$ is part of a hexagonal grid. Depending on the state of the fluid parcel at (i,j), A^k_{ij}, can take three possible values, $A^k_{i,j} = 1$ for unburned gas parcel, $A^k_{i,j} = 2$ for burning flamelet and $A^k_{i,j} = 3$ for burned gas parcel. Note that these specific values are only representative and can be chosen differently. Each step of cellular automata is evolved using the algorithm given in Eq. (1). The algorithm uses a set of relational operators, explained below. == represents the operator *equal to*, where $X == a$ outputs a matrix Y (with same dimensions as X), in which $Y_{i,j} = 1$ if $X_{i,j} == a$, else $Y_{i,j} = 0$. $\circ$ represents the Hadamard product operator, such that $(X \circ Y)_{i,j} = X_{i,j}Y_{i,j}$. $S[\cdot]$ is a filter operator defined such that $S[X == \eta]_{i,j}$ outputs the total number of neighbors of $X_{i,j}$ which has a value equal to η. In this work, considering that the grid topology is hexagonal, the six neighbors of $X_{i,j}$ are $X_{i-1,j+1}, X_{i-1,j}, X_{i,j-1}, X_{i,j+1}, X_{i+1,j-1}$ and $X_{i+1,j}$. Based on these operators, the evolution equation for A^k can be expressed as

$$A^{k+1} = T_1 + T_2 + T_3 + T_4, \tag{1}$$

where

$$T_1 = 3 \times (A^k == 3), \tag{R1}$$

$$T_2 = 3 \times (A^k == 2), \tag{R2}$$

$$T_3 = 2 \times (A^k == 1) \circ (\Gamma \leq Q) \circ (S[A^k == 2] > 0), \tag{R3}$$

$$T_4 = -1 \times (A^k == 2) \circ (\Gamma \leq R) \circ (S[A^k == 1] > 0). \tag{R4}$$

The term T_1 corresponds to Rule 1 of cellular automata. The term T_2 corresponds to Rule 2, T_3 corresponds to Rule 3, and T_4 corresponds to Rule 4. Here, Γ is a matrix with dimensions same as that of A^k and each element of which is a random number from 0 to 1 uniformly distributed in that range. An operation $\Gamma \leq \beta$ outputs a binary matrix, κ, of same dimensions as that of Γ, such that $\kappa_{i,j} = 1$ if $\Gamma_{i,j} \leq \beta$, else $\kappa_{i,j} = 0$.

The wrinkling of turbulent flames causes the surface area of the flame to increase proportional to $\tilde{R}^H$, where $\tilde{R}$ is the average radius of the wrinkled flame (radius of a sphere that has an equivalent volume as contained within the wrinkled surface of the turbulent flame) and H is the fractal dimension of the wrinkled flame surface. This power law variation of surface area with $\tilde{R}$ results in $\tilde{R}(t)$ varying proportional to t^α, fractal excess, where $\alpha = \frac{1}{3-H}$.[23,24] In the present model, each time step of the cellular automaton, dt, results in the flamelet propagating across a single cell. Each time step, dt, is a constant and is normalized with the time taken for a laminar flamelet to travel a distance equal to the laminar flame thickness, δ_l. So, in order to capture this power law variation of $\tilde{R}(t)$ vs t, we vary the size of the hexagonal grid, l non-linearly with each time step dt of the cellular automaton (note that dt is a unit time), such that $l = \frac{d\tilde{R}}{dt} \times dt = \delta_l \alpha t^{\alpha-1}$. In the model, clearly, α is a function of P. For simplicity, we consider that for $t > 1$, $\alpha - 1 = P$, and hence for the laminar case ($P = 0$), $l = \delta_l$. As P increases, l varies non-linearly with respect to time so that acceleration of the turbulent expanding flamefront is captured.

III. RESULTS AND DISCUSSION

A. Flame dynamics

In this section, we will examine some of the key behaviors of the expanding turbulent flames, modeled using cellular automata. In

the low order model introduced in Sec. II, an increase in turbulence level of the flow field is captured by increasing P; however, we note that the dependence between P and U_{rms} velocity of turbulent flow field is not necessarily linear in nature. Recognizing that the propagation and characteristics of expanding flames are highly affected by the turbulence level, we report its effect on three flame characteristics, namely, flame morphology, flame surface area, and flame speed. Flame morphology can be extracted by plotting the instantaneous locations of flamelets (or burning cells) at different time instances for various turbulence levels or P (Fig. 2). To examine the instantaneous flame surface area, we compare the quantity $q(t)$, defined as the length of the flamefront or the total number of flamelets over the domain at time step t, for various P [Fig. 3(a)]. Since turbulence is intermittent in nature, which introduces fluctuations in the instantaneous value of $q(t)$, we also evaluate its ensemble average of $\langle q(t)\rangle$, whose time derivative, $\langle \dot{q}(t)\rangle$, is proportional to the global flame speed or the burning rate [Fig. 3(b)]. Here, $\langle q(t)\rangle$ is obtained by averaging 400 realizations of $q(t)$.

For laminar condition, corresponding to $P = 0$, the flame is seen to expand uniformly in all directions [Figs. 2(a)–2(d)]. Since we have used a hexagonal grid over which the cellular automaton is defined, and in each step of the cellular automaton, the flamefront propagates by one grid, the flame assumes a hexagonal shape. We find $q(t)$ and $\langle q(t)\rangle$ both change linearly with t and the slope is six (Fig. 3) for $P = 0$. Since we have not included any differential diffusion or Lewis number effect, the propagation speed or rate of increase in flame surface area is supposed to be constant, which results in a linear slope.

As we introduce a moderate level of turbulence by increasing P to 0.45, the flamefront starts to wrinkle due to the effect of turbulent eddies, which is captured by the model, as seen in Figs. 2(e)–2(h) for $P = 0.45$. We observe that inherent "randomness" in turbulence removes the effect of grid shape, in that the flame loses the initial hexagonal shape. Due to its inherent spatial intermittency, introduction of turbulence also induces strong fluctuations in $q(t)$ (Fig. 3), which, however, vanishes for the ensemble quantity, $\langle q(t)\rangle$ (Fig. 3). It is noted that $\langle q(t)\rangle$ for $P = 0.45$ is higher than that of $P = 0$ for any time instance, which is caused by the augmented flame surface area due to wrinkling. For laminar ($P = 0$) and turbulent ($P = 0.45$) conditions, one can further compare the slope of $\langle q(t)\rangle$ and $d\langle q(t)\rangle/dt$, which is equivalent of the burning rate. The curves in Fig. 3(b) clearly show that $d\langle q(t)\rangle/dt$ for $P = 0.45$ is higher than that of the laminar case ($P = 0$), suggesting enhanced flame speed due to turbulence. Moreover, for the turbulent condition $P = 0.45$, the slope of the curves seems to increase with time, suggesting an acceleration of turbulent expanding flame as it propagates. Both these observations corroborate observations from numerous experiments.[7,20,25] On further increase in the turbulence level or P, at $P = 0.53$ the flamefront starts becoming disconnected [Figs. 2(i)–2(l)]. This is an artifact of local extinction pertaining to stronger flame straining. As a consequence of these random local flame holes or extinctions and subsequent re-connections or re-ignitions, we observe larger fluctuations in $q(t)$ at $P = 0.53$ compared to those for the lower level of turbulence at $P = 0.45$ [Fig. 3(a)]. Furthermore, the intermittent occurrence of flame holes reduce the average burning rate causing the average slope of $\langle q(t)\rangle$ vs t for a given t to reduce.

As turbulence is increased further, at $P = 0.54$, the expanding flame starts to fragment into multiple disconnected flamefronts [Figs. 2(m)–2(p)] as occurrence of local extinctions become higher due to increased local straining. The increased level of turbulence also causes the active flamefronts to become extremely wrinkled. We observe that the fluctuations in $q(t)$ reduce compared to that for $P = 0.53$ [Fig. 3(a)], owing to reduced probability of flame propagation ($1 - P$) and the increased number of flame holes compared to lower turbulence levels. Turbulence induced local quenching and fragmentation of the flame leading to weakened burning is reported in Yang *et al.*[8] At very high turbulence levels, the local quenching can lead to global extinction of the flame.

At $P = 0.55$, the turbulence is high enough to quench the flame at its nascent state [Fig. 2(q)–2(t)]. Correspondingly, we can see that the $q(t)$ fluctuates and then goes to zero [zoomed in view in the inset of Fig. 3(a)]. Also, the ensemble averaged flamelet population $\langle q(t)\rangle$ shows an initial increase and eventual decay to zero [zoomed in view in the inset of Fig. 3(b)]. Such quenching of flame kernels after ignition was reported in experiments by multiple groups.[26–30]

B. Fractal analysis

The dynamics and propagation of a flame is largely governed by the topology of the flamefront. Recognizing that turbulence inherently exhibits fractal behavior, the topology of an evolving flamefront in a turbulent flow field is often characterized by its fractal characteristics.[31,32] However, in cellular automaton, turbulence is modeled using a the probability of flame propagation that has a Gaussian white noise distribution and by definition is not necessarily fractal in nature. Emergence of fractal topology in the turbulent flamefront obtained from this model would imply that such a low-order description can capture the proper description of turbulent flame propagation and as such can be used as a low-order model to study certain aspects of turbulent flames. To assess the complete scaling behavior of the system, we construct a multifractal spectrum corresponding to the simulated flamefront topology reported in Sec. III A. The complete description of multifractal models in lights of an expanding turbulent flame can be found in Saha *et al.*[33] Here, we briefly summarize the important variables. Multifractal spectrum or singularity spectrum of a fractal function, $g(x)$, describes the complete set of fractals that constitute the function $g(x)$.[34] Multifractal spectrum $f(\alpha)$ of $g(x)$ is the Hausdorff dimension for the manifold formed by all x, which has a singularity of α. Here, $f(\alpha)$ is also known as the singularity strength. In this study, we estimate the multifractal spectrum using the box-counting method.[34]

Figure 4(a) shows the multifractal spectrum for the flamefront with an average radius, $\tilde{R} = 25$ for single realizations of expanding flamefronts obtained for different values of P. $\tilde{R}$ for the cellular automata model is estimated as the average distance of flamelets from the center of the grid normalized with the grid size. When $P = 0$, the flamefront is hexagonal in nature and hence not fractal. For small turbulence levels corresponding to $P = 0.10$, the multifractal spectrum has a finite width. The finite width of the multifractal spectrum is indicative of the wrinkling of the flame surface and the presence of multiple fractal scaling in the topology of the flame. As the turbulence level increases, for $P = 0.45$, the multifractal spectrum width increases and the spectrum moves to the right

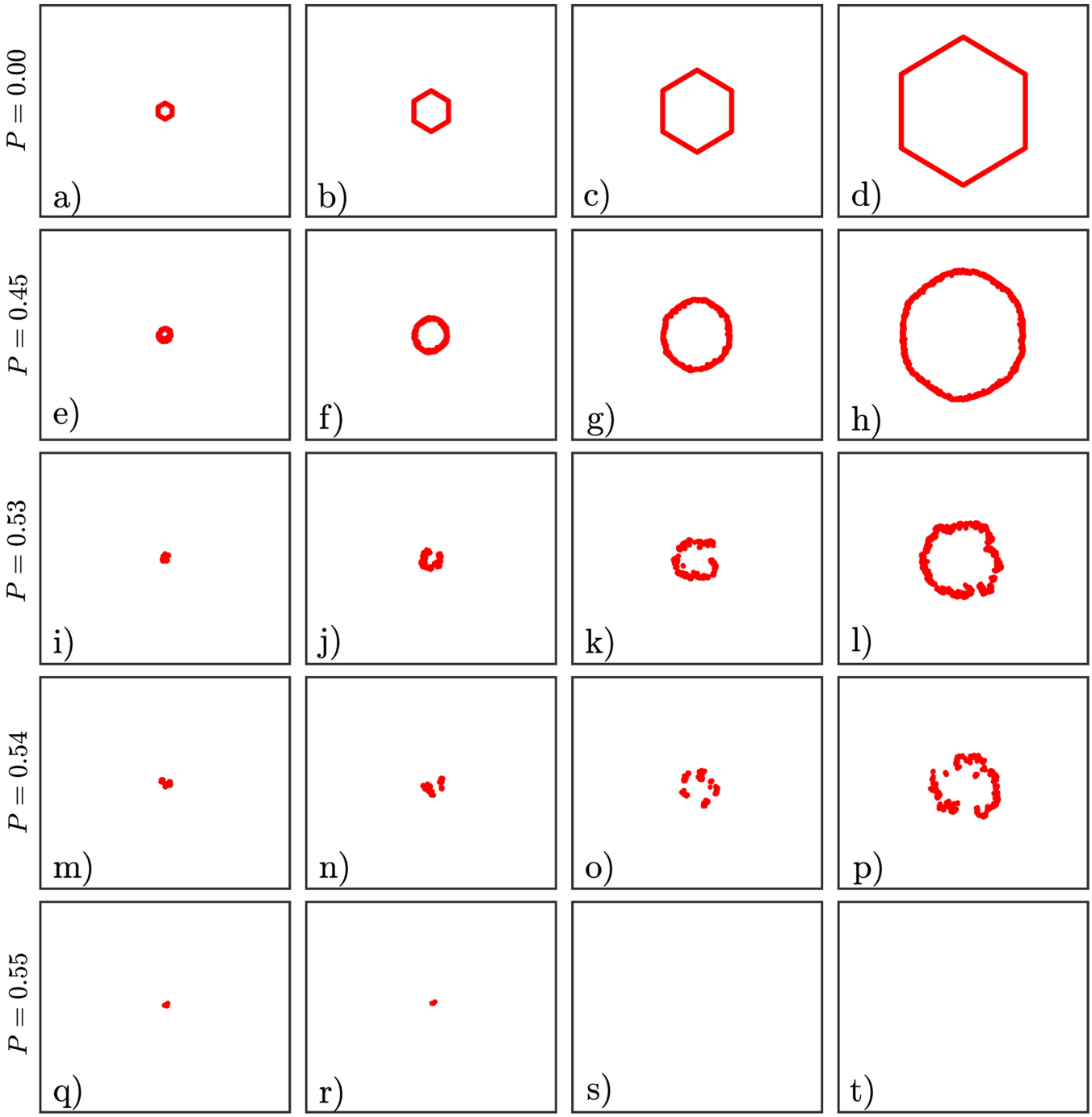

FIG. 2. Expanding flame at different levels of turbulence (represented by P) is shown in different rows. Different column represents different time instants during the expansion of the spherical flame. (a)–(d) corresponds to $P = 0$, i.e., laminar conditions. (e)–(h) corresponds to $P = 0.45$, Here, the turbulence causes the flamefront to wrinkle. (i)–(l) corresponds to $P = 0.53$; due to increased turbulence, the flame develops intermittent flame holes and is highly wrinkled. (m)–(p) corresponds to $P = 0.54$. The flame is fragmented leading to disconnected flamefronts. (q)–(t) corresponds to $P = 0.55$. Here, the very high turbulence causes the flame to extinguish at nascent stage.

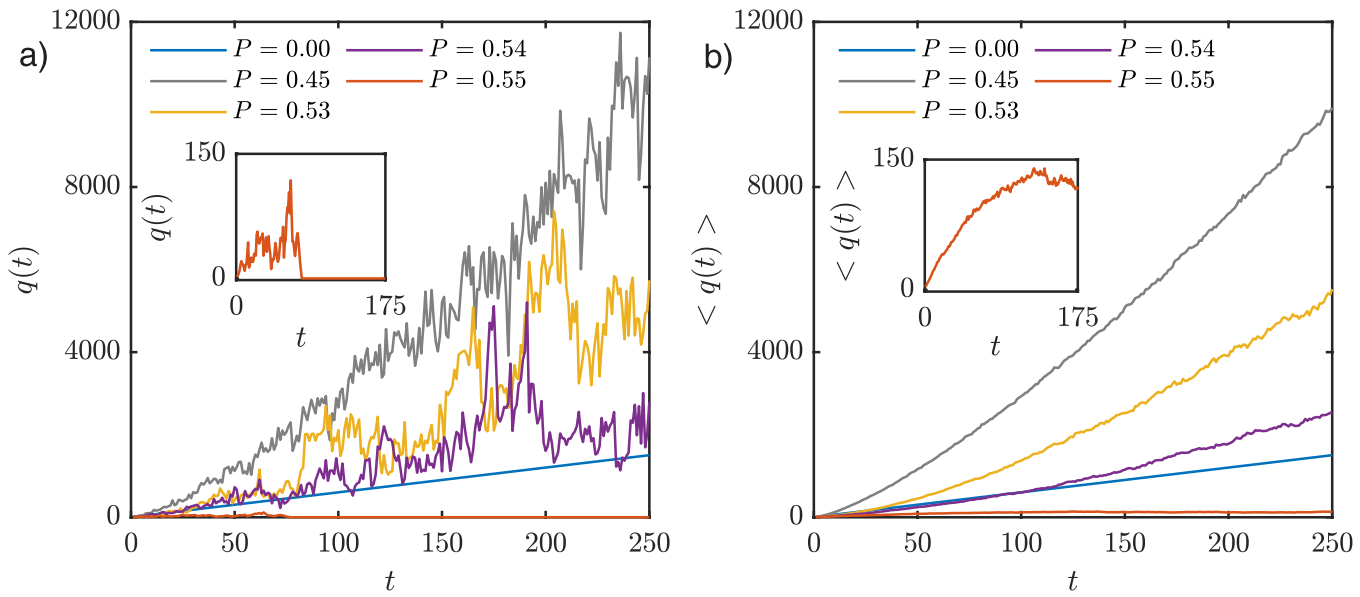

FIG. 3. (a) Flamelet population $q(t)$ with time for different values of P for one realization. (b) $\langle q(t) \rangle$, the ensemble average of $q(t)$ for different values of P. $\langle q(t) \rangle$ is obtained by averaging $q(t)$ over 400 realizations. Note that here t represents the temporal steps of the cellular automaton and, hence, has an arbitrary unit.

top corner. This is indicative of an increase in the fractal dimension of the flame due to enhanced wrinkling of the flame surface and an increase in the range of singularities in the topology of the flame. The increase in the width of multifractal spectrum implies that additional scales have been added to the process of flame wrinkling, while the movement of the spectrum toward right suggests that the new fractal scales that were added to the topology have higher fractal dimension and, hence, increasingly more finer wrinkles. Similar observations

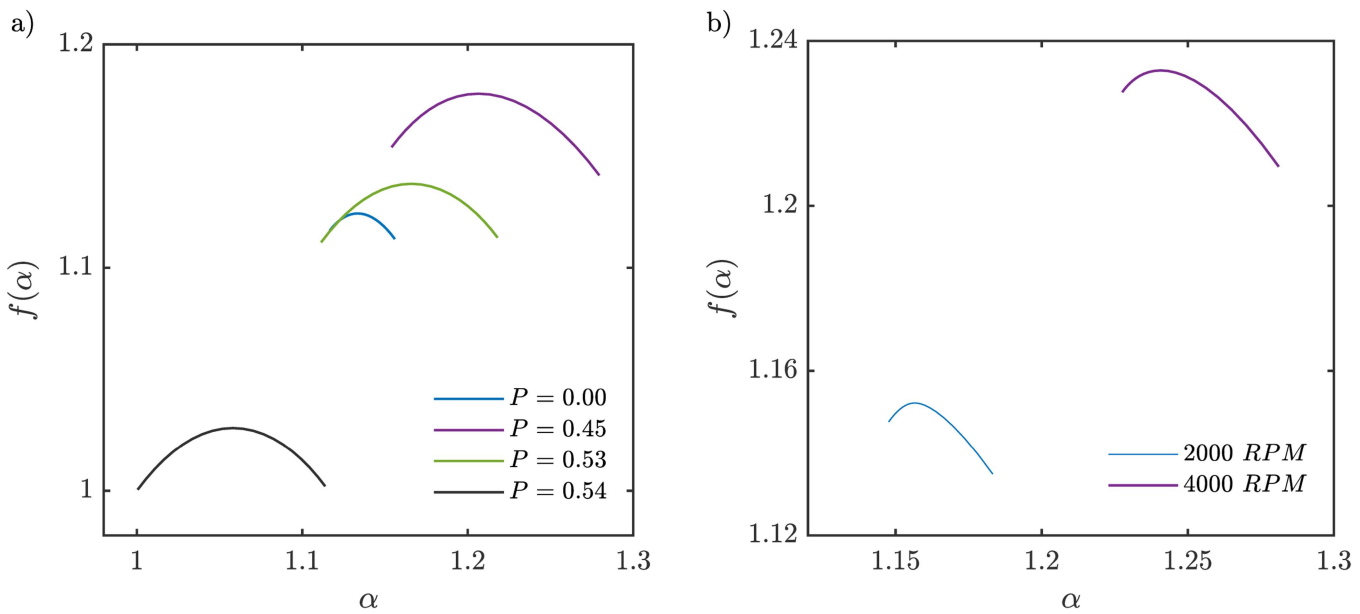

FIG. 4. (a) Multifractal spectrum corresponding to flamefronts for which $\tilde{R} = 25$ for different values of turbulence levels (P) obtained from the cellular automata model. (b) Multifractal spectrum corresponding to expanding flames with $\tilde{R} = 9.5$ mm obtained from experiments.

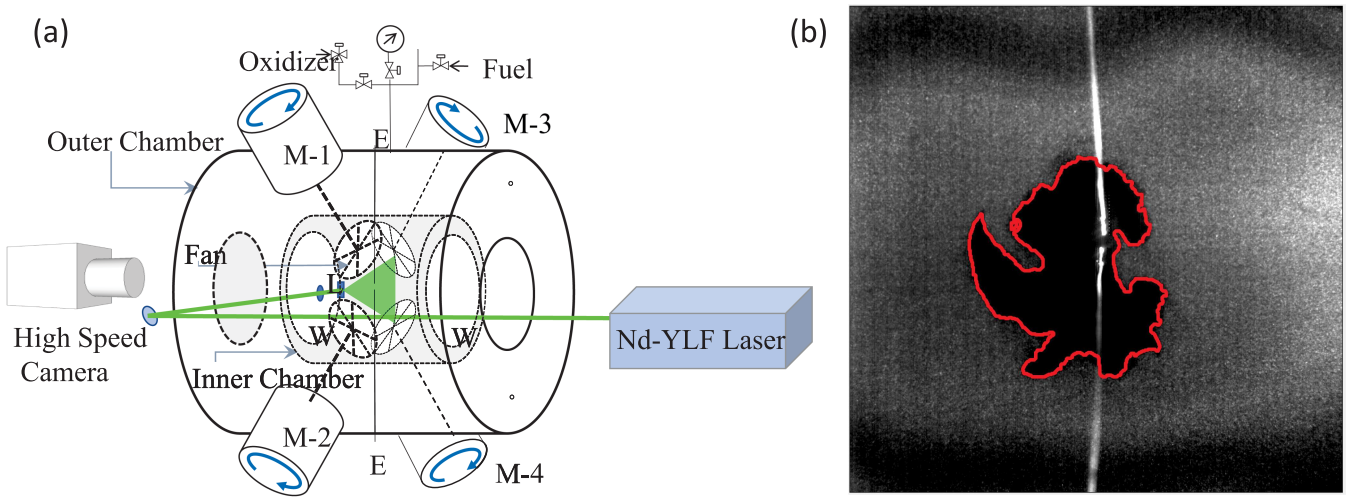

FIG. 5. (a) Schematic of the experimental setup used for studying turbulent expanding flame.[20] (b) A typical Mie-scattering image and detected flame edge.

have been reported in experiments by Saha *et al.*[33] They showed that as turbulence intensity is increased, the multifractal spectrum representing the topology of the flame shifts to the right and the spectrum width increases. However, since they were using multifractal detrended fluctuation analysis, they were not able to capture the increase in the singularity strength of the spectrum as the turbulence level was changed. In the present study, we use the box counting method to obtain the multifractal spectrum of the flamefront. Hence, we are able to capture both the change in the multifractal spectrum width and the change in the range of singularity strength of the spectrum for the topology of flame surface as the turbulence level is varied.

In the model, we see that when the turbulence level is further increased, at $P = 0.53$, both the width of the spectrum and the maximum singularity strength in the spectrum, $\max(f(\alpha))$ reduces. This is caused by local extinction, flame holes, and resultant reduction in the average burning rate at higher turbulence level as seen in Figs. 2 and 3. Further increase in P causes the flame to fragment into multiple disjoined flamefronts causing further reduction in the range of singularity strengths and range of singularities that describe the flame topology. The multifractal spectrum also shifts to the left indicating a reduction in small wrinkles in the flame topology. Beyond this turbulence level, the flame extinguishes in its nascent stage.

To qualitatively compare the fractal dimensions of the flamefront based on our model, we analyzed the data from experiments reported in Saha *et al.*[33] These experiments were conducted in a dual-chambered vessel in which the propagation of a spark-ignited expanding flame can be studied under constant pressure.[7,8] In the experiments, the flame propagated in a nearly isotropic homogeneous turbulent flow field, which was generated by four orthogonally located continuously rotating fans.[7,20] Before the experiment, a mixture of methane (CH_4) and air with appropriate proportions was introduced into the chamber to obtain a mixture with an equivalence ratio of 0.9. The mixture was further seeded with micrometer-sized DEHS droplets. A high-speed Nd-YLF laser along with relevant optics was used to generate a thin 2D laser sheet at the center of the chamber. A high-speed camera synchronized with the laser pulses was used to capture the Mie-scattering images from the droplets, which evaporate near the flame edge leaving a trace of the flamefront. Using these high-speed images, evolution of the flamefront of the expanding flame propagating in turbulent environment could be studied. The experimental setup and a sample Mie-scattering image are shown in Fig. 5. The Mie-scattering images were analyzed using the box-counting method to obtain the multifractal spectra.

Here, we consider flames at two turbulence levels, the lower one corresponds to a fan rotational speed of 2000 RPM ($U_{rms} \approx 1.17$ m/s) and the higher one corresponds to a fan rotational speed of 4000 RPM ($U_{rms} \approx 2.34$ m/s). The fractal characteristics of these expanding flames are then compared for similar radius, $R \approx 9.5$ mm and shown in Fig. 4(b). For experiments, R is the radius of a circle that encompasses the same area as enclosed by the fractal flamefront. The multifractal spectrum obtained from the experimental data is indeed qualitatively similar with that from the model. Specifically, we observe that the multifractal spectrum from experiments with higher turbulence level has a higher maximum value and is shifted to the right, as it was the case for data based on the model.

IV. CONCLUSIONS

We introduced a probabilistic cellular automaton to model the population dynamics of flamelets in a turbulent field. The model was able to qualitatively reproduce various dynamical aspects of an expanding turbulent flame. It was seen that a moderate increase in turbulence leads to an increase in the average burning rate accompanied with the wrinkling of flamefront. When turbulence was increased beyond a certain limit the flame exhibited flame holes and the average burning rate reduced. Further increase in turbulence led to the fragmentation of the flame and at highest turbulence levels,

the flame extinguished in its nascent state. The model was also able to capture the multifractal characteristics of the turbulent flames, suggesting that such models could be used as low-order models for describing the spatiotemporal dynamics of turbulent flames.

We end this exposition by acknowledging that the proposed model based on cellular automata does not directly involve the generalized combustion equations used for premixed flames. However, the four rules that we used to construct the proposed model include the elements of transport and propagation of the flamefront and its interaction with the neighboring fluid elements. It can be shown that such cellular automata can be analogous to level-set based formulations, such as well-known G-equation, used in combustion, albeit with its inherent simplicity and assumptions.

ACKNOWLEDGMENTS

The authors are grateful to Professor Swetaprovo Chaudhuri (University of Toronto) for encouragement and technical comments on the manuscript. The work at Princeton was supported by the US National Science Foundation (CBET, Grant No. 1827287). A.S. acknowledges UCSD's internal grants for providing financial support for the research.

DATA AVAILABILITY

The data that support the findings of this study are available from the corresponding author upon reasonable request.

REFERENCES

[1]S. Pope, "The evolution of surfaces in turbulence," Int. J. Eng. Sci. **26**, 445–469 (1988).
[2]N. Peters, *Turbulent Combustion*, Cambridge Monographs on Mechanics (Cambridge University Press, 2000).
[3]C. K. Wu and C. K. Law, "On the determination of laminar flame speeds from stretched flames," in *Symposium (International) on Combustion* (Elsevier, 1985), Vol. 20, pp. 1941–1949.
[4]C. K. Law and C. J. Sung, "Structure, aerodynamics, and geometry of premixed flamelets," Prog. Energy Combust. Sci. **26**, 459–505 (2000).
[5]C. K. Law, *Combustion Physics* (Cambridge University Press, 2006).
[6]A. P. Kelley and C. K. Law, "Nonlinear effects in the extraction of laminar flame speeds from expanding spherical flames," Combust. Flame **156**, 1844–1851 (2009).
[7]S. Chaudhuri, F. Wu, D. Zhu, and C. K. Law, "Flame speed and self-similar propagation of expanding turbulent premixed flames," Phys. Rev. Lett. **108**, 044503 (2012).
[8]S. Yang, A. Saha, W. Liang, F. Wu, and C. K. Law, "Extreme role of preferential diffusion in turbulent flame propagation," Combust. Flame **188**, 498–504 (2018).
[9]Z. Liu, S. Yang, C. K. Law, and A. Saha, "Cellular instability in Le< 1 turbulent expanding flames," Proc. Combust. Inst. **37**, 2611–2618 (2018).
[10]F. Creta, R. Lamioni, P. E. Lapenna, and G. Troiani, "Interplay of Darrieus–Landau instability and weak turbulence in premixed flame propagation," Phys. Rev. E **94**, 053102 (2016).
[11]G. Troiani, F. Creta, and M. Matalon, "Experimental investigation of Darrieus–Landau instability effects on turbulent premixed flames," Proc. Combust. Inst. **35**, 1451–1459 (2015).
[12]S. Wolfram, "Cellular automata as models of complexity," Nature **311**, 419–424 (1984).
[13]A. López-Martín, P. L. García-Ybarra, J. L. Castillo, and J. C. Antoranz, "Self-turbulent flame simulation by a cellular automaton," in *IUTAM Symposium on Variable Density Low-Speed Turbulent Flows* (Springer, 1997), pp. 59–62.
[14]P. L. García-Ybarra, J. C. Antoranz, and J. L. Castillo, *Growth and Form* (Springer, 1991). pp. 253–259.
[15]R. Said and R. Borghi, "A simulation with a "cellular automaton" for turbulent combustion modelling," in *Symposium (International) on Combustion* (Elsevier, 1989), Vol. 22, pp. 569–577.
[16]S. D. Tse, D. L. Zhu, and C. K. Law, "Morphology and burning rates of expanding spherical flames in H_2/O_2/inert mixtures up to 60 atmospheres," Proc. Combust. Inst. **28**, 1793–1800 (2000).
[17]D. R. Dowdy, D. B. Smith, S. C. Taylor, and A. Williams, "The use of expanding spherical flames to determine burning velocities and stretch effects in hydrogen/air mixtures," in *Symposium (International) on Combustion* (Elsevier, 1991), Vol. 23, pp. 325–332.
[18]R. Mével, F. Lafosse, N. Chaumeix, G. Dupré, and C.-E. Paillard, "Spherical expanding flames in H_2–N_2 O–Ar mixtures, flame speed measurements and kinetic modeling," Int. J. Hyd. Energy **34**, 9007–9018 (2009).
[19]S. Chaudhuri, F. Wu, and C. K. Law, "Scaling of turbulent flame speed for expanding flames with markstein diffusion considerations," Phys. Rev. E **88**, 033005 (2013).
[20]S. Chaudhuri, A. Saha, and C. K. Law, "On flame–turbulence interaction in constant-pressure expanding flames," Proc. Combust. Inst. **35**, 1331–1339 (2015).
[21]R. Abdel-Gayed, D. Bradley, and M. Lawes, "Turbulent burning velocities: A general correlation in terms of straining rates," Proc. R. Soc. Lond. A **414**, 389–413 (1987).
[22]V. R. Unni, S. Chaudhuri, and R. I. Sujith, "Flame blowout: Transition to an absorbing phase," Chaos **28**, 113121 (2018).
[23]M. A. Liberman, M. F. Ivanov, O. E. Peil, D. M. Valiev, and L.-E. Eriksson, "Self-acceleration and fractal structure of outward freely propagating flames," Phys. Fluids **16**, 2476–2482 (2004).
[24]S. Yang, A. Saha, F. Wu, and C. K. Law, "Morphology and self-acceleration of expanding laminar flames with flame-front cellular instabilities," Combust. Flame **171**, 112–118 (2016).
[25]J. Goulier, A. Comandini, F. Halter, and N. Chaumeix, "Experimental study on turbulent expanding flames of lean hydrogen/air mixtures," Proc. Combust. Inst. **36**, 2823–2832 (2017).
[26]A. Saha, S. Yang, and C. K. Law, "On the competing roles of turbulence and differential diffusion in facilitated ignition," Proc. Combust. Inst. **37**, 2383–2390 (2018).
[27]C. F. Kaminski, J. Hult, M. Aldén, S. Lindenmaier, A. Dreizler, U. Maas, and M. Baum, "Spark ignition of turbulent methane/air mixtures revealed by time-resolved planar laser-induced fluorescence and direct numerical simulations," Proc. Combust. Inst. **28**, 399–405 (2000).
[28]D. Bradley, C. G. W. Sheppard, I. M. Suardjaja, and R. Woolley, "Fundamentals of high-energy spark ignition with lasers," Combust. Flame **138**, 55–77 (2004).
[29]S. F. Ahmed, R. Balachandran, and E. Mastorakos, "Measurements of ignition probability in turbulent non-premixed counterflow flames," Proc. Combust. Inst. **31**, 1507–1513 (2007).
[30]S. S. Shy, C. C. Liu, and W. T. Shih, "Ignition transition in turbulent premixed combustion," Combust. Flame **157**, 341–350 (2010).
[31]A. R. Kerstein, "Fractal dimension of turbulent premixed flames," Combust. Sci. Tech. **60**, 441–445 (1988).
[32]F. C. Gouldin, "An application of fractals to modeling premixed turbulent flames," Combust. Flame **68**, 249–266 (1987).
[33]A. Saha, S. Chaudhuri, and C. K. Law, "Flame surface statistics of constant-pressure turbulent expanding premixed flames," Phys. Fluids **26**, 045109 (2014).
[34]A. Chhabra and R. V. Jensen, "Direct determination of the f(α) singularity spectrum," Phys. Rev. Lett. **62**, 1327 (1989).